

# Dynamic Covalent Bond-Assisted Programmed and Traceless Protein Release: High Loading Nanogel for Systemic and Cytosolic Delivery

Shan Su, Yao-Yi Wang, Fu-Sheng Du,\* Hua Lu,\* and Zi-Chen Li

Systemic and cytosolic delivery represents a grand challenge preventing many therapeutic proteins from clinical applications. Despite tremendous progresses in the past decade, most approaches generally lack the ability of triggered traceless protein release, require complicated formulation, and/or yield low protein loading. By using the protein as a crosslinker, here, a simple and general formulation affording protein nanogels (NG) with uniformed sizes and exceptionally high protein loading (>50%) is reported. By using the fine-tuned bis- and monosubstituted maleamic anhydride-amine chemistry for the crosslinking of the protein and a 4-armed PEG-MA<sub>4</sub>, the NG is implemented with a tandem pH-programmed and traceless release character. The final NG, CDM-MA-NG, is stable under normal physiological conditions and effectively protects the crosslinked cargo cytochrome C from serum fouling, proteolytic and thermal degradation. In vitro, CDM-MA-NG exhibits a high level of cellular uptake and potent cancer cell killing only when incubated at pH 6.5, but not 7.4. Systemic administration of CDM-MA-NG leads to significantly inhibited tumor growth and extended survival rate. Given the abundance of the amine groups on protein surface, this work describes a universal platform for therapeutic protein formulation, and opens up enormous opportunities for the systemic, cytosolic, and traceless delivery of protein-based nanomedicines.

## 1. Introduction


Protein therapeutics play important and versatile roles in disease treatment, prevention, and health promotion.<sup>[1]</sup> Compared to small molecular drugs, protein drugs frequently enjoy unique advantages such as high specificity and high potency. However, the in vivo applications of protein drugs are largely prevented by their short circulation, rapid degradation, and low cellular membrane permeability.<sup>[2]</sup> To overcome these issues, various

delivery approaches have been developed. One approach relies on the covalent modification of proteins. For instance, the vast success of protein PEGylation has been exemplified by the more-than-a-dozen approved drugs.<sup>[3]</sup> Often, the proteins are covalently modified via amine-*N*-hydroxy succinimide (NHS),<sup>[4]</sup> thiol-maleimide,<sup>[5]</sup> or glutaraldehyde chemistries.<sup>[6]</sup> Nevertheless, these permanent chemical modifications require time-consuming synthetic endeavors and often lead to irreversibly reduced biological activity. One vivid example is the more than 90% activity loss in Pegasys, a PEGylated interferon- $\alpha$ 2a approved in 2001 for treating hepatitis.<sup>[7]</sup> On the contrary, another approach capitalizes on various physical associations to load the protein cargo in nano-sized carriers including liposomes,<sup>[8]</sup> polymersomes,<sup>[8a,9]</sup> gold nanoparticles,<sup>[10]</sup> mesoporous silica nanoparticle,<sup>[11]</sup> and nanogels (NG).<sup>[12]</sup> However, many of those methods suffer from complicated formulation, low drug loading, premature cargo release, loss of protein activity, and carrier-

induced toxicity. Indeed, the vast majority of physically encapsulated delivery systems can only reach  $\approx$ 10% protein loading or less. In this regard, many systems are not suitable for in vivo uses, especially when systemically administrated. Moreover, because of the contradictory requirements posed by the complex biological barriers to the design of nanomedicine,<sup>[13]</sup> very few examples, regardless the covalent or noncovalent approach, can realize efficient systemic and cytosolic protein delivery.<sup>[14]</sup> As a result, only those proteins do not require an intracellular mechanism of action are currently used in clinic. To this end, one unmet need is a simple formulation simultaneously enabling high protein loading, outstanding stability under physiological conditions, and most importantly, a traceless release character in the cytoplasm.<sup>[12b,14–16]</sup>

Instead of physically encapsulating or covalently attaching the cargo protein into certain carriers, we envisage that the in situ crosslinking of proteins with a polyethylene glycol (PEG) crosslinker via dynamic covalent bonds (DCB) may yield responsive protein NGs with all the desired properties, particularly the high loading. We further reason that the acid-sensitive and reversible maleamic anhydride-amine chemistry<sup>[17]</sup> is ideal for the crosslinking. First of all, the abundant

S. Su, Y.-Y. Wang, Prof. F.-S. Du, Prof. H. Lu, Prof. Z.-C. Li  
Beijing National Laboratory for Molecular Sciences  
Key Laboratory of Polymer Chemistry & Physics of Ministry of Education  
Department of Polymer Science & Engineering  
College of Chemistry and Molecular Engineering  
Center for Soft Matter Science & Engineering  
Peking University  
Beijing 100871, P. R. China  
E-mail: fsdu@pku.edu.cn; chemhualu@pku.edu.cn

 The ORCID identification number(s) for the author(s) of this article can be found under <https://doi.org/10.1002/adfm.201805287>.

DOI: 10.1002/adfm.201805287

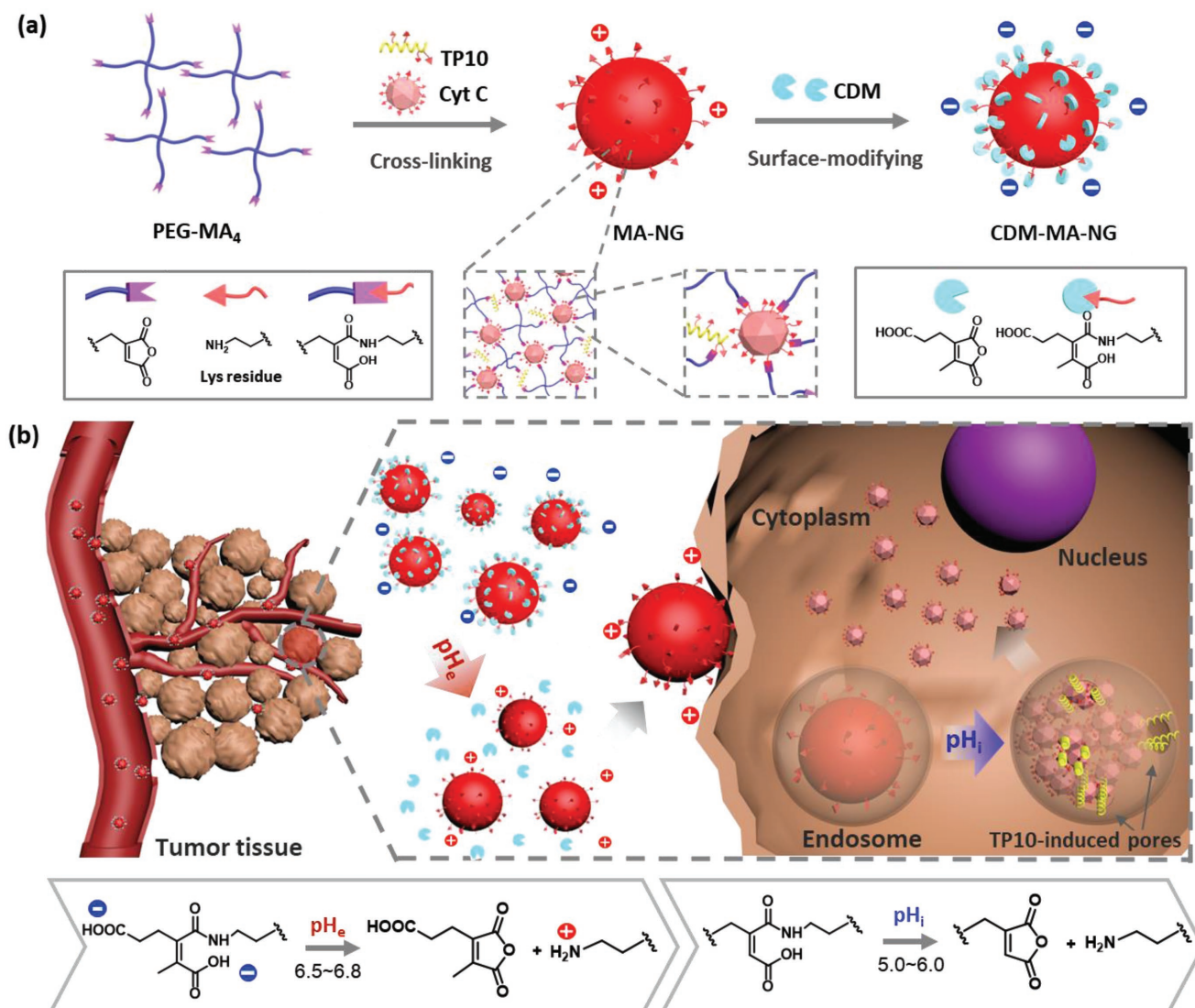


**Figure 1.** Design and synthesis of the tandem pH-responsive nanogel CDM-MA-NG. a) Two-step preparation of the nanogel CDM-MA-NG. b) Cartoon illustration of the systemic administrated CDM-MA-NG for enhanced intracellular and traceless delivery of Cyt C via a tandem pH-triggered NG decomposition mechanism. Mono- and bisubstituted maleamic anhydride derivatives show pH-responsive hydrolysis at pH<sub>i</sub> and pH<sub>e</sub>, respectively.

lysine amines can readily react with the maleamic anhydride (MA) to achieve sufficiently high protein loading; the generated carboxylic acid, together with the PEG corona, can collectively form a stealthy shell at physiology pH. Second, the hydrolysis of the maleamic acid bond, promoted by the adjacent carboxylic acid at slightly lower pH, can regenerate the protein in its native form. Third, we have recently shown that the onset pH of the maleamic amide hydrolysis can be precisely adjusted to both the extracellular tumor microenvironment (pH<sub>e</sub>, ≈6.5–6.8) and the intracellular late endosome (pH<sub>i</sub>, ≈5.0–6.0) by using bis- and monosubstituted MA derivatives, respectively (Figure 1).<sup>[17a,18]</sup> Thus, the introduction of both bis- and monosubstituted MA in the NG allows programmed cargo release responding to tandem pH changes.<sup>[14,18,19]</sup> Previously, MA derivatives have been widely used as charge inversion moieties in nanomedicines facilitating enhanced tumor retention and cellular uptake at tumor microenvironment.<sup>[19]</sup>

For instance, Kataoka and co-workers reported the modification of cytochrome C (Cyt C) and IgG with a monosubstituted MA, and its subsequent formulation with a cationic polymer to generate polyionic complexes (PICs). In vitro, the PICs were efficiently internalized due to its positive charges, and the cargo proteins were released in a traceless way upon acidification in lysosome. However, the in vivo application of the PICs was not reported possibly due to the low protein loading and the instability of the electrostatic interaction.<sup>[19a,20]</sup> Of note, only the pH<sub>i</sub>-responsive monosubstituted MA was used in the system.

Herein, we report the rapid construction of a Cyt C nanogel, denoted as CDM-MA-NG, by successively crosslinking and modifying lysine amines with both mono- and bisubstituted maleamic anhydrides (Figure 1). CDM-MA-NG features in exceptionally high protein loading content (≈51% loading by weight), and is stable under normal physiological conditions

without serum protein fouling. **CDM-MA-NG** is designed to undergo rapid charge inversion at the slightly acidic tumor microenvironment  $pH_e$  for tumor internalization, and release Cyt C in a traceless fashion upon further acidification at the endosomal  $pH_i$ . In vitro, **CDM-MA-NG** exhibits high therapeutic index evidenced by the extremely low toxicity at  $pH$  7.4, and the highly effective cancer cell killing at  $pH_e$  (6.5). In vivo, **CDM-MA-NG** shows exceptionally high antitumor efficacy upon tail vein administration without systemic toxicity and side effects.

## 2. Results and Discussion

### 2.1. Preparation and Characterization of NGs

Cyt C was chosen as a model protein drug because of its sufficient amino groups (19 lysine units) and high positive charge density (+1391 Da per charge).<sup>[19a]</sup> Previously, Cyt C was identified as an important apoptosis mediator activating the downstream caspase pathway, only when released from mitochondria to cytoplasm. However, its in vivo therapeutic potential was prevented from the lack of appropriate cytosolic delivery method.<sup>[20,21]</sup> To promote the intracellular delivery, a lysine-rich cell-penetrating peptide, transportan 10 (TP10, sequence: LIKKALAALAKLNKGLLYGA),<sup>[22]</sup> was introduced for coformulation with Cyt C. The nanogel **CDM-MA-NG** was prepared by a simple two-step process (Figure 1b): (1) the in situ crosslinking of Cyt C/TP10 mixture with a 4-arm-PEG bearing four mono-substituted maleic anhydride (molecular weight 5 kDa, PEG-MA<sub>4</sub>), and (2) the surface masking of remaining lysines with

a bis-substituted maleic anhydride (carboxy-dimethylmaleic anhydride, CDM).

For this, we first synthesized the crosslinker PEG-MA<sub>4</sub> from PEG-OH<sub>4</sub> as shown in Figure S1 in the Supporting Information. The chemical structure of PEG-MA<sub>4</sub> was confirmed by NMR and GPC with modification ratio up to 85% (Figures S2–S4, Supporting Information). Model reactions of PEG-MA<sub>4</sub> or CDM with *n*-butylamine were performed to test the reactivity of the pairs in water. Remarkably, the reaction of PEG-MA<sub>4</sub> with *n*-butylamine completed within 5 min (Figure S6, Supporting Information). For the reaction of CDM with *n*-butylamine, a relative more basic aqueous solution ( $pH > 9$ ) and a large excess of CDM appeared crucial to ensure complete transformation of *n*-butylamine (Figure S7, Supporting Information). Both model reactions were highly efficient and incredibly clean without sign of side reactions, laying the foundation for protein nanogel synthesis in water.

Next, an aqueous solution containing Cyt C and TP10 was nanoprecipitated in an acetonitrile solution containing PEG-MA<sub>4</sub> to afford the crosslinked **MA-NG** (Figure 1a). After a brief optimization of the formulation conditions (Table S1 Supporting Information), **MA-NG** was purified by dialysis against a sodium bicarbonate solution. Dynamic light scattering (DLS) measurements of **MA-NG** showed a mean diameter of 133 nm (Figure S8, Supporting Information) and fluorescamine labeling indicated that  $\approx 73\%$  primary amine of Cyt C and TP10 remained intact (Figure 2a; Figure S9, Supporting Information). To cap the rest lysine residues, excessive CDM was added to **MA-NG** to afford **CDM-MA-NG**. Titration of the primary amine revealed only  $\approx 2.2\%$  lysine unreacted after this step (Figure 2a; Figure S9, Supporting Information). **CDM-MA-NG**

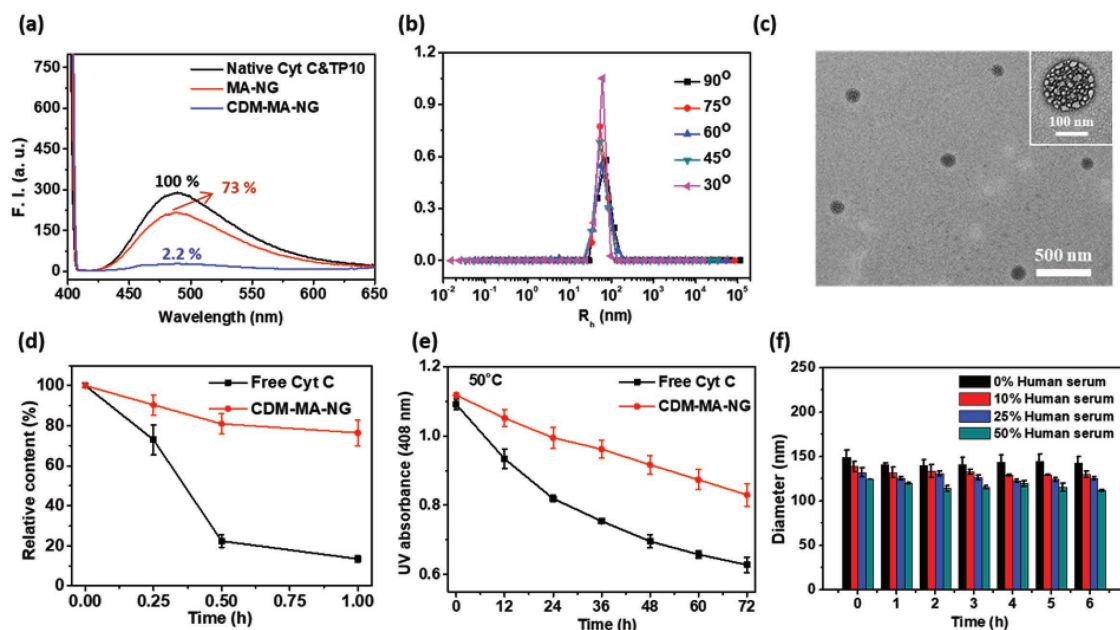


**Figure 2.** Characterization and stability of **CDM-MA-NG**. a) Fluorescence spectra of fluorescamine with native Cyt C & TP10 (Cyt C/TP10 ratio is 1:1), **MA-NG** and **CDM-MA-NG** ( $\lambda_{ex} = 397$  nm). b) Size distribution of **CDM-MA-NG** in PBS ( $pH$  7.4,  $20 \times 10^{-3}$  M) at  $37$  °C. c) TEM image of **CDM-MA-NG**. d) Degradation of free and crosslinked Cyt C by trypsin (0.5 equiv.) at  $37$  °C. e) Stability of free and crosslinked Cyt C upon  $50$  °C incubation assessed by the UV absorption at 408 nm. f) Particle size of **CDM-MA-NG** in the diluted (0%, 10%, 25%, and 50%) human blood serum (Cyt C conc:  $0.4$  mg mL<sup>-1</sup>). All experiments were repeated as triplicates, and data are presented as means  $\pm$  standard deviations.

had a diameter of 140 nm by DLS, similar to that of MA-NG (Figure 2b; Figure S10, Supporting Information). TEM further confirmed the size of CDM-MA-NG was  $\approx 150$  nm with a spherical shape (Figure 2c). With the successful modification of CDM, the zeta potential of the NG dropped from the original +1.3 to  $-27$  mV. Remarkably, the final protein loading efficiency (PLE) and protein loading contents (PLC) of the two-step process was 71% and 51%, respectively, both are remarkably high as compared to most current protein-based nanomedicines.<sup>[23]</sup> Following the same procedure, two control NGs were prepared for comparison purpose. Namely, a non-pH<sub>e</sub>-sensitive SA-MA-NG was produced by modifying MA-NG with succinic anhydride (SA), and a non-pH<sub>i</sub>-sensitive CDM-NHS-NG was synthesized by crosslinking Cyt C and TP10 using PEG-NHS<sub>4</sub> and followed by CDM surface masking (Figure S11, Supporting Information).

## 2.2. Stability of CDM-MA-NG

Chemical modification was well-known to impart the conjugated protein improved thermostability and protease resistance.<sup>[24]</sup> To test whether Cyt C in CDM-MA-NG was stabilized from degradation, free Cyt C and CDM-MA-NG were separately incubated with protease (i.e., trypsin), or at high temperature (50 °C) for 72 h. As shown in Figure 2d and Figure S12 (Supporting Information), less than 25% Cyt C in CDM-MA-NG was affected after 1 h trypsin treatment, whereas more than 80% degradation under the same condition was observed for free Cyt C. This excellent proteolytic resistance of CDM-MA-NG relative to free Cyt C was probably due to the chemically blocked lysine residues and increased steric hindrance.<sup>[24b,25]</sup> Similarly, protein denature by heat was also effectively retarded by immobilizing Cyt C in the network of CDM-MA-NG (Figure 2e). To further

examine the stealth effect, the size of CDM-MA-NG was measured with the addition of human serum over a period of 6 h (Figure 2f). No change in the size of the NGs was observed throughout the study, implying that the CDM masking and PEG prevented serum protein binding. The superior stability of CDM-MA-NG under normal physiological conditions thus strongly favored its systemic administration in live animals.

## 2.3. pH Sensitivity of CDM-MA-NG

To study the programmed response of the NGs in circulation, tumor issues, and intracellular environment, we monitored the zeta potential and size of the NGs at pH 7.4, 6.5, and 5.5, respectively. As shown in Figure 3a, CDM-MA-NG kept a negatively charged surface with the zeta potential of  $\approx -22.3$  mV for 3 h at pH 7.4; while the zeta potential of CDM-MA-NG quickly increased to +1.5 and +6.6 mV at pH 6.5 and 5.5, respectively. In contrast, the non-pH<sub>e</sub>-sensitive SA-MA-NG gave almost no changes in zeta potential in the tested pH range (Figure 3b). To further study the dynamic surface charge inversion of CDM-MA-NG, the solution was slowly titrated with  $100 \times 10^{-3}$  M HCl (Figure S13, Supporting Information). Along with the gradient reduction of the pH, the zeta potential of CDM-MA-NG rose from the initial  $-25.0$  mV to the first plateau of +2.2 mV at pH 6.5, and followed by a further boost to the second plateau of +6.3 mV at pH 5.5 (Figure 3c).

We next employed laser light scatter (LLS) to study the size change of CDM-MA-NG responding to pH fluctuation. Figure 3d–f and Figure S14 (Supporting Information) show the changes in scattered light intensity, hydrodynamic radius ( $R_h$ ), and radius of gyration ( $R_g$ ) as a function of time. The scattered light intensity of CDM-MA-NG remained unchanged at pH 7.4 and decreased slowly by 31% in the course of 24 h

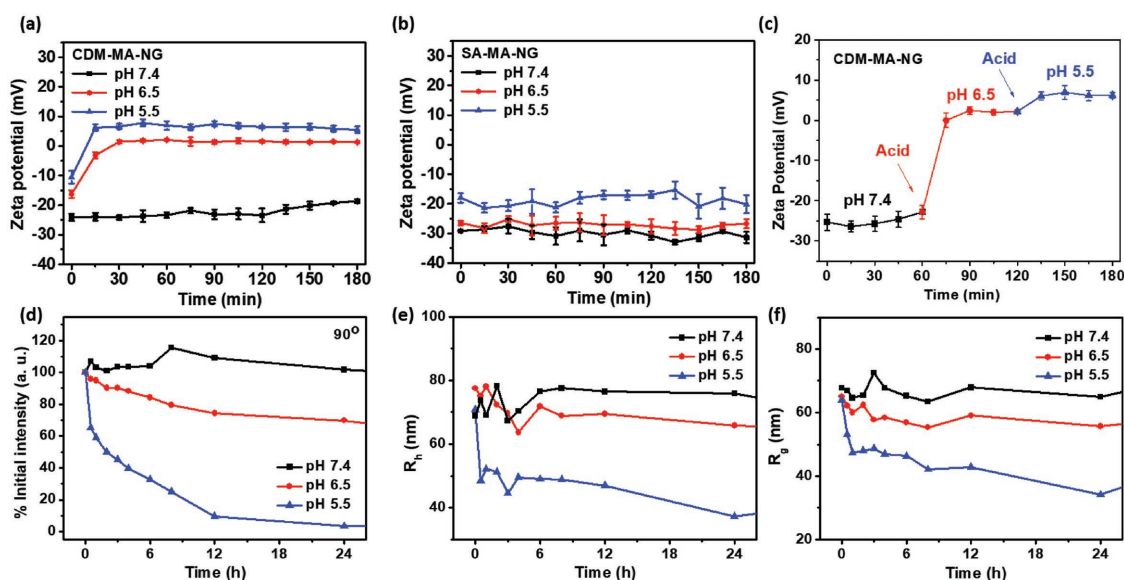


**Figure 3.** Tandem pH-responsiveness of CDM-MA-NG. Zeta potential changes of a) CDM-MA-NG and b) SA-MA-NG (Cyt C  $0.2 \text{ mg mL}^{-1}$ ) when incubated in PBS (pH 7.4, 6.5 or 5.5,  $20 \times 10^{-3}$  M) for different time periods. c) Change of zeta potential of CDM-MA-NG (Cyt C  $0.2 \text{ mg mL}^{-1}$ ) along with gradient decrease of the pH value from 7.4 to 6.5 and 5.5. Time-dependent changes of d) scattered light intensity, e)  $R_h$ , and f)  $R_g$  of CDM-MA-NG (Cyt C  $0.1 \text{ mg mL}^{-1}$ ) at pH 7.4, 6.5, or 5.5; the NG was incubated with PBS at 37 °C.

at pH 6.5. A more significant reduction of the scattered light intensity at pH 5.5 implied that **CDM-MA-NG** completely decomposed over the detection time (Figure 3d). Moreover, LLS of **CDM-MA-NG** showed continuous decline in  $R_h$  and  $R_g$  as the solution was acidified (Figure 3e,f). Interestingly, the control group **CDM-NHS-NG** did not display noticeable changes on neither the scattered light intensity nor the size under the same experimental conditions (Figures S15 and S16, Supporting Information).

#### 2.4. Traceless Release of Cyt C from CDM-MA-NG

Next, we investigated the acid-triggered release of Cyt C from **CDM-MA-NG** by placing the NG in a dialysis bag (COMW  $\approx$ 300 kDa) at 37 °C and measuring the releasing Cyt C based on the heme absorption in the solution outside the dialysis bag. Incubation of the NG with phosphate buffer saline (PBS) led to very few Cyt C release at pH 7.4, and the total amount of released protein only increased marginally at pH 5.5. On the contrary, when the pH was further decreased to 5.5, the same NG released 38%, 80%, and 95% Cyt C at 6, 12, and 24 h, respectively (Figure 4a). This was in good consistency with the fact that the hydrolysis of the monosubstituted maleic amide was slow above pH 6.5 but fast at pH 5.5 (half-life at pH 6.5 is  $\approx$ 31 times of that at pH 5.5).<sup>[17b]</sup> To verify whether Cyt C was released in a traceless fashion, matrix-assisted laser desorption/ionization time of flight mass spectrometry (MALDI-TOF-MS), circular dichroism (CD) spectroscopy, and an enzyme activity assay were performed (Figure 4b–d). MALDI analysis confirmed that the released protein had a consistent  $m/z$  with

that of the native Cyt C, a strong support of the traceless release (Figure 4b). The CD spectra of native and the released Cyt C showed an almost perfect coincidence from 200 to 500 nm, suggesting both the tertiary structure of Cyt C and the heme cofactor were preserved during the treatment (Figure 4c; Figure S17, Supporting Information). More importantly, ABTS assay<sup>[26]</sup> (see the Supporting Information) displayed essentially identical kinetics for native and the released Cyt C (Figure 4d). The results implied that the protein was functionally intact following the whole process of nanoprecipitation, in situ crosslinking, and in vitro release.

#### 2.5. Cellular Uptake Measured by Flow Cytometry and Confocal Laser Scanning Microscopy

To test whether **CDM-MA-NG** can give more efficient internalization at tumor microenvironment than in circulation, we compared the cellular uptake of **CDM-MA-NG** and **SA-MA-NG** (Cyt C were fluorescein isothiocyanate (FITC)-labeled) at pH 7.4 and 6.5. As shown in Figure 5a and Figure S18a (Supporting Information), flow cytometry indicated that the uptake of **CDM-MA-NG** was significantly higher at pH 6.5 than neutral pH. As expected, the internalization of the control group **SA-MA-NG** was pH-independent and substantially lower than that of **CDM-MA-NG**. Moreover, a clear time-dependent uptake of **CDM-MA-NG** by HeLa cells was observed in the course of 48 h at pH 6.5 (Figure 5b).

The cellular uptake and distribution of NGs were further evaluated by confocal laser scanning microscopy (CLSM, Figure 5c; Figures S18b and S19, Supporting Information) in

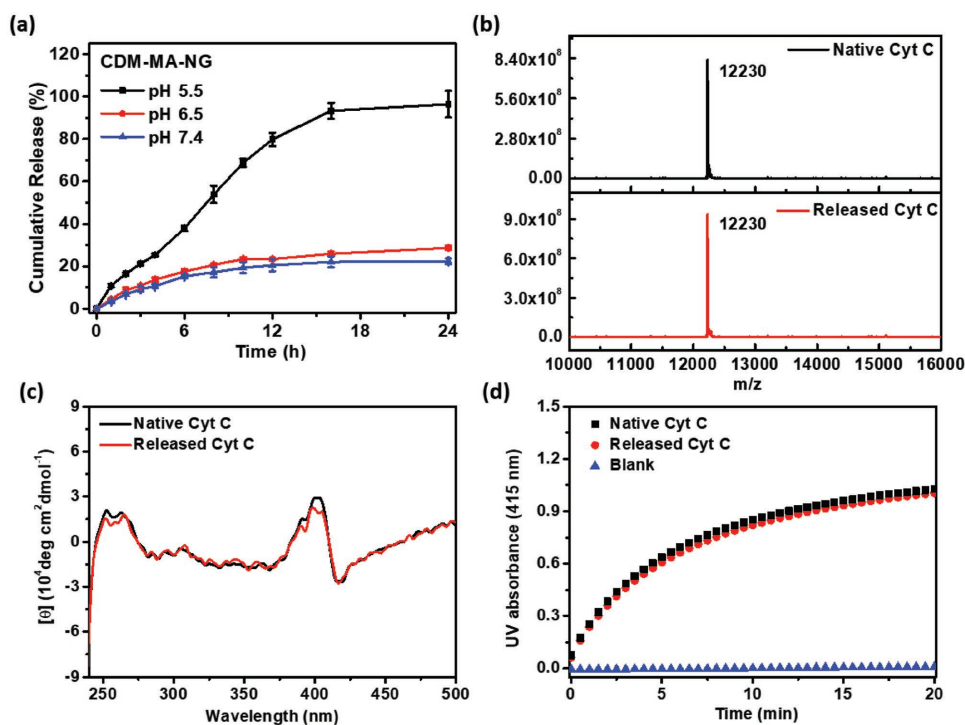


**Figure 4.** Traceless Release of Cyt C from **CDM-MA-NG** at pH<sub>i</sub>. a) Release profile of Cyt C from the **CDM-MA-NG** in PB (pH 7.4, 6.5 or 5.5,  $20 \times 10^{-3}$  M) at 37 °C. b) MALDI-MS spectra, c) CD spectroscopy, and d) ABTS activity assay of the native Cyt C and released Cyt C from **CDM-MA-NG**.

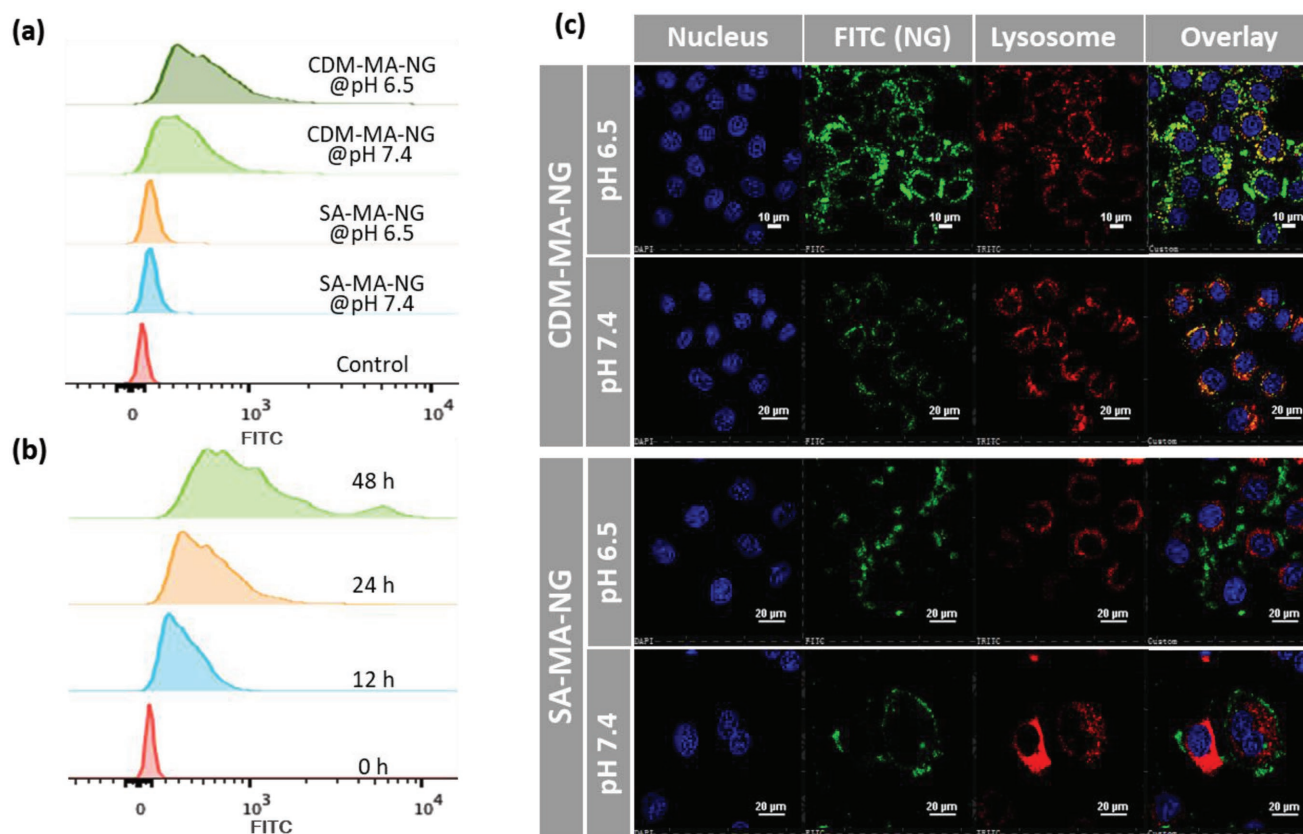


**Figure 5.** pH- and time-dependent cellular uptake of CDM-MA-NG. a) Flow cytometry analysis of the pH-dependent cellular uptake of FITC-labeled **CDM-MA-NG** and **SA-MA-NG**; the NGs were incubated with HeLa cells at pH 7.4 or 6.5 for 24 h. b) Flow cytometry analysis of time-dependent cellular uptake of FITC-labeled **CDM-MA-NG** at pH 6.5. c) CLSM images of the pH-dependent cellular uptake of **CDM-MA-NG** and **SA-MA-NG**; the NGs were incubated with HeLa cells at pH 7.4 or 6.5 for 24 h. Cyt C was fixed at  $25 \mu\text{g mL}^{-1}$  for all studies.

HeLa cells. Incubation of **CDM-MA-NG** at pH 6.5 exhibited the strongest intracellular fluorescence of FITC among all groups. Colocalization study of the NGs with lysosome indicated that a small portion of Cyt C escaped from the lysosome after 24 h incubation, which was likely assisted by the released TP10 at  $\text{pH}_i$ . The internalization of the identical NG was rarely observed when incubated at pH 7.4. Compared with **CDM-MA-NG**, however, **SA-MA-NG** revealed poor cellular uptake ability at both pH 7.4 and 6.5. Collectively, all results corroborated the remarkable  $\text{pH}_e$ -assisted internalization of **CDM-MA-NG** and  $\text{pH}_i$ -assisted endosomal escape. Notably, **CDM-MA-NG** without TP10 failed to give satisfactory cellular uptake and endosomal release under the tested conditions (Figure S20, Supporting Information).

## 2.6. In Vitro Anticancer Activity of CDM-MA-NG

The antitumor activity of **CDM-MA-NG** was investigated by incubating the NG with HeLa cells at pH 7.4 or 6.5 (Figure 6). At pH 7.4, none of the treatment induced noticeable cytotoxicity after 72 h incubation and the cell viability of all groups were over 90% even at the highest concentration tested. When the cells were incubated at pH 6.5, **CDM-MA-NG** showed prominent cytotoxicity with a  $\text{IC}_{50}$  value of  $12 \mu\text{g mL}^{-1}$ , whereas neither native Cyt C nor the control **SA-MA-NG** treatment displayed detectable cell

killing (Figure 6a). Thus, this result suggested that **CDM-MA-NG** would be safe in circulation and highly effective at cancer killing once reaching the tumor microenvironment. Of note, none of the components used in the NGs including the crosslinker (PEG-MA<sub>4</sub>), the shield (CDM), and the cell penetrating peptide (TP10) showed detectable toxicity to HeLa cells under the same conditions (Figure 6b; Figure S21, Supporting Information), suggesting that the cell killing effect of **CDM-MA-NG** was predominantly derived from the released Cyt C. To confirm that the NGs-induced cell death was indeed apoptosis, we assessed the apoptotic activity of **CDM-MA-NG** by using flow cytometry (Figure 6c; Figure S22, Supporting Information). After incubation of the materials at pH 6.5 or 7.4, the HeLa cells were stained with apoptotic markers such as Annexin V-FITC and PI. Flow cytometry analysis indicated that the dual pH sensitive **CDM-MA-NG** exhibited substantial apoptotic activity after as early as 24 h incubation, and the fractions of apoptotic cells were considerably higher at pH 6.5 than those at pH 7.4. In contrast, very few apoptotic cells were observed in the non- $\text{pH}_e$ -sensitive **SA-MA-NG** group under both pH 6.5 and 7.4 conditions.

It has been reported that Cyt C must be translocated to the cytoplasm to induce activation of apoptotic downstream effectors, and free Cyt C was ineffective because of low cellular uptake and poor endosomal escape.<sup>[21a]</sup> Here, the extensive cell apoptosis provoked by **CDM-MA-NG** at pH 6.5 unambiguously

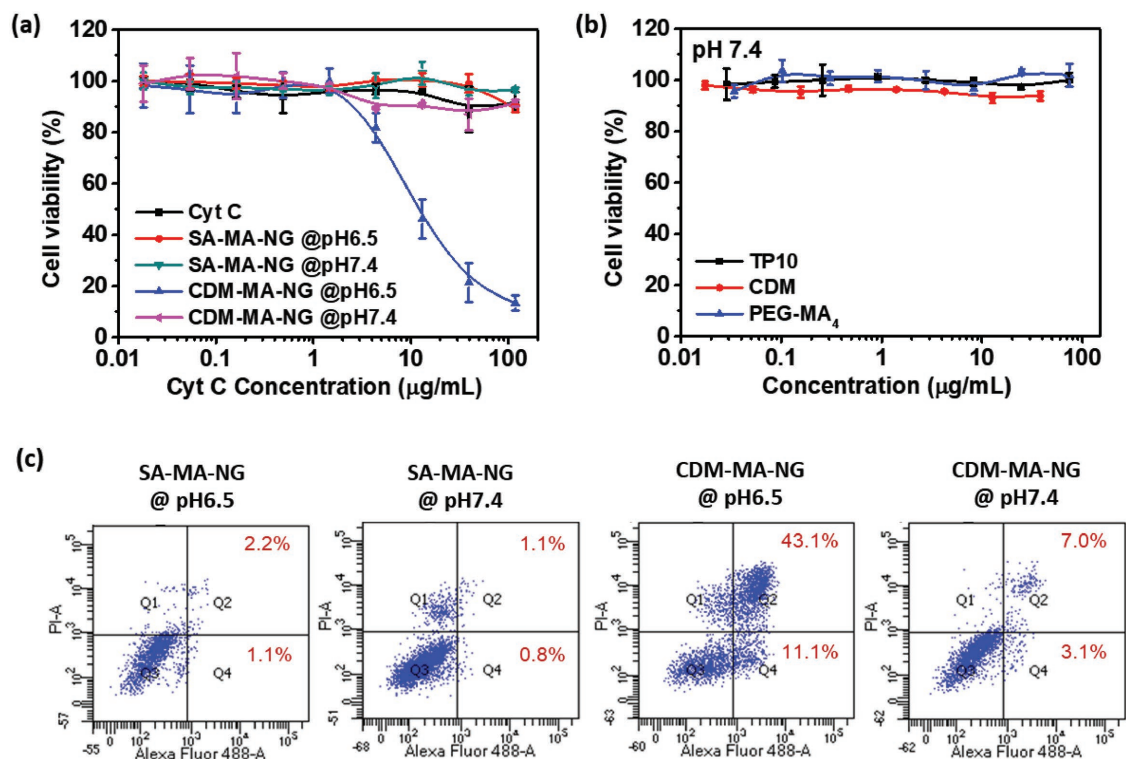


**Figure 6.** In vitro cytotoxicity and cell apoptosis induced by CDM-MA-NG. pH-dependent cytotoxicity of a) free Cyt C and Cyt C-loaded NGs, and b) TP10, CDM, and PEG-MA<sub>4</sub>. HeLa cells were incubated with the materials at pH 6.5 or 7.4 for 72 h, and the relative viability was measured by MTT assay. c) Flow cytometry contour diagram analysis of cell apoptosis; HeLa cells were incubated with Cyt C-loaded NGs (Cyt C 25 µg mL<sup>-1</sup>) at pH 6.5 or 7.4 for 24 h, and stained with Annexin V-FITC/PI.

pointed out that the NG was not only efficiently internalized through the pH<sub>e</sub>-facilitated charge inversion, but also effectively released Cyt C in its functional form to cytoplasm. This was likely via the pH<sub>i</sub>-triggered collapse of the NG, which released the cell-penetrating peptide TP10 for enhanced endosomal escape.<sup>[22]</sup>

## 2.7. In Vivo Therapeutic Efficacy

To investigate the in vivo biosafety and antitumor efficacy of CDM-MA-NG, we established a HeLa xenograft model in Balb-c/nude mice. The mice with tumor volume of ≈50 mm<sup>3</sup> were randomly divided and intravenously infused with PBS, Cyt C, SA-MA-NG, and CDM-MA-NG (200 µg Cyt C/kg) every other day, respectively. At the end of the treatment, on day 26, the tumors in mice receiving both PBS and Cyt C outgrew exponentially (≈60–70 fold increase), and SA-MA-NG only marginally inhibited the tumor growth (≈51 fold increase). In sharp contrast, the administration of CDM-MA-NG showed very effective tumor growth inhibition with the tumor size augmented only approximately six times (Figure 7a). Remarkably, the antitumor efficacy of CDM-MA-NG still persisted even after discontinuation of the treatment (Figure 7a). As expected, CDM-MA-NG treatment also significantly extended the survival rate (SR) of the tumor-bearing mice with a 100% SR on day 40, as compared to 0% on day 30 for all other groups (Figure 7b). No body weight loss was observed for all treatments (Figure 7c). Furthermore,

we investigated the tumor inhibition with histology analysis of the extracted tumor tissues via both Ki-67 and H&E staining method. The CDM-MA-NG treated group showed less Ki-67 stained cells (Figure 7d) and more empty holes (Figure 7e, yellow arrows), which indicated more effective inhibition of cancer cell proliferation and a higher degree of tumor damages by the pH sensitive nanogel. Overall, these results were in consistent with the tumor volume progression.

The in vivo safety of CDM-MA-NG was evaluated by performing blood biochemical analysis and histological studies. According to the histology results, no organ damages were found in heart, kidney, spleen, and lung for all treatments. Interestingly, lymphocyte infiltration in the liver, likely due to long-term tumor burden, was observed at the end of the study for mice treated with PBS, free Cyt C, and SA-MA-NG, but not in those receiving CDM-MA-NG (Figure 7f). Measurement of biochemical parameters such as blood urea nitrogen (BUN), alkaline phosphatase (ALP), aspartate transaminase (AST), lactate dehydrogenase (LDH), and alanine transaminase (ALT) all gave results within the normal ranges (Figure S21, Supporting Information), suggesting the excellent biosafety of CDM-MA-NG.

## 3. Conclusion

In conclusion, we reported a simple and general formulation yielding tandem pH-sensitive and charge-reversal nanogel

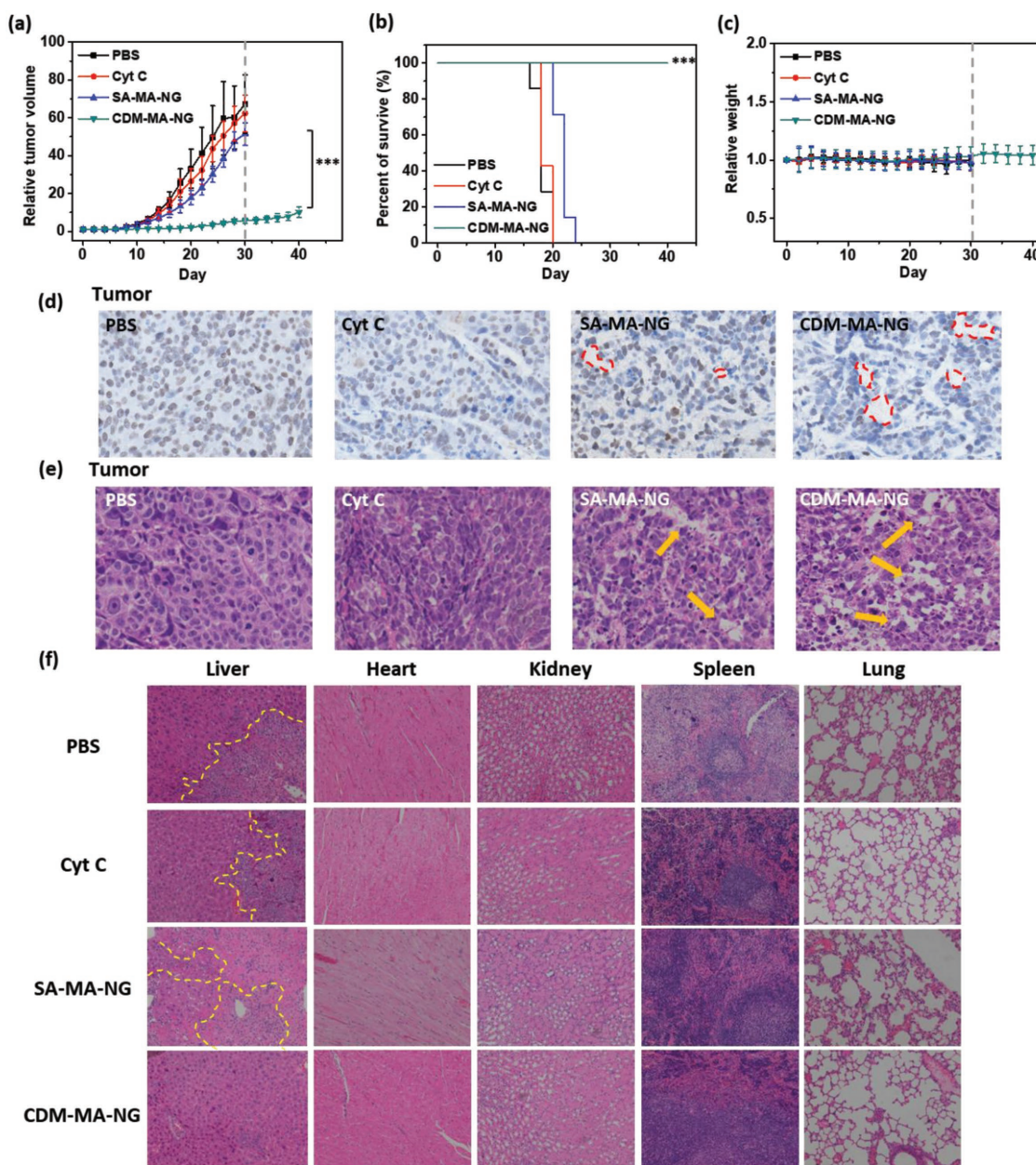


**Figure 7.** In vivo antitumor efficacy of Cyt C-loaded NGs. a) Tumor growth inhibition curve, b) survival rate curve, and c) body weight curve of HeLa tumor-bearing mice receiving PBS saline, Cyt C, SA-MA-NG, or CDM-MA-NG ( $n = 7$ ). d) Ki67- and e) H&E-stained tumor sections, and f) H&E-stained major organs sections such as liver, heart, kidney, spleen, and lung dissected from mice on day 30. BALB/C-nu mice bearing s.c. HeLa tumor ( $\approx 50 \text{ mm}^3$ ) were i.v. injected with PBS saline or Cyt C-based therapies at  $200 \mu\text{g kg}^{-1}$  every other day; therapies started on day 0 and stopped on day 30 (grey dashed line in a and c); natural decease or mice with more than 15% body weight loss or  $1000 \text{ mm}^3$  tumors were all counted as mice death in the SR curves; red dash lines in inset (d) and the yellow arrows in inset (e) point out damaged tumor tissues; yellow dash lines in inset (f) indicate the lymphocyte infiltration areas. Data are expressed as means  $\pm$  SD;  $p$  value was determined by two-way ANOVA analysis:  $*p < 0.05$ ,  $**p < 0.01$ ,  $***p < 0.001$ .

CDM-MA-NG for the systemic and cytosolic delivery of functional proteins in vivo. The formulation did not require genetic engineering or premodification of the protein, making it readily applicable to many other therapeutic proteins. The protein loading of CDM-MA-NG easily reached more than 50%, with a 71% loading efficiency. CDM-MA-NG showed remarkable high thermostability, and outstanding resistance toward protease degradation and serum protein fouling. Under normal conditions, CDM-MA-NG kept a size of 150 nm with a PEG

corona and a negative zeta-potential, making it “invisible” in circulation. At tumor microenvironment, CDM-MA-NG was rapidly degraded due to the slightly acidic  $\text{pH}_e$ -induced CDM hydrolysis, and the exposed lysine amine led to enhanced tumor retention and cellular internalization. The NG automatically fall apart upon further acidification to  $\text{pH}_i$  in lysosome, releasing Cyt C and TP10 in cytoplasm in a traceless fashion. Due to this intelligent and programmed responsiveness, CDM-MA-NG showed exceptional efficacy including high levels



of cell apoptosis in vitro and remarkable inhibition of tumor growth in vivo without detectable side effects. Given the generality and robustness of the method, this work may open up enormous opportunities for the efficient systemic and cytosolic delivery of protein-based nanomedicines.

## Supporting Information

Supporting Information is available from the Wiley Online Library or from the author.

## Acknowledgements

S.S. and Y.W. contributed equally to this work. This work was financially supported by National Key Research and Development Program of China (No. 2016YFA0201400) and National Natural Science Foundation of China (Nos. 21534001 and 21722401).

## Conflict of Interest

The authors declare no conflict of interest.

## Keywords

cytochrome C, high loading, maleamic acids, nanogels, tandem pH responsiveness, traceless protein delivery

Received: July 31, 2018  
Revised: September 20, 2018  
Published online:

- [1] B. Leader, Q. J. Baca, D. E. Golan, *Nat. Rev. Drug Discovery* **2008**, 7, 21.
- [2] a) Z. Gu, A. Biswas, M. Zhao, Y. Tang, *Chem. Soc. Rev.* **2011**, 40, 3638; b) S. Mitragotri, P. A. Burke, R. Langer, *Nat. Rev. Drug Discovery* **2014**, 13, 655; c) M. Yu, J. Wu, J. Shi, O. C. Farokhzad, *J. Controlled Release* **2016**, 240, 24.
- [3] R. Duncan, F. M. Veronese, in *PEGylated Protein Drugs Basic Science and Clinical Applications* (Ed: F. M. Veronese), Vol. 1, Birkhäuser, Basel **2009**, pp. 1–288.
- [4] a) D. Mertz, H. Wu, J. S. Wong, J. Cui, P. Tan, R. Alles, F. Caruso, *J. Mater. Chem.* **2012**, 22, 21434; b) M. Morales-Cruz, A. Cruz-Montanez, C. M. Figueroa, T. Gonzalez-Robles, J. Davila, M. Inyushin, S. A. Loza-Rosas, A. M. Molina, L. Munoz-Perez, L. Y. Kucheryavykh, A. D. Tinoco, K. Griebenow, *Mol. Pharmaceutics* **2016**, 13, 2844.
- [5] a) K.-C. Kao, C.-H. Lee, T.-S. Lin, C.-Y. Mou, *J. Mater. Chem.* **2010**, 20, 4653; b) R. Ohri, S. Bhakta, A. Fourie-O'Donohue, J. dela Cruz-Chuh, S. P. Tsai, R. Cook, B. Wei, C. Ng, A. W. Wong, A. B. Bos, F. Farahi, J. Bhakta, T. H. Pillow, H. Raab, R. Vandlen, P. Polakis, Y. Liu, H. Erickson, J. R. Junutula, K. R. Kozak, *Bioconjugate Chem.* **2018**, 29, 473.
- [6] W. Tong, C. Gao, H. Moehwald, *Colloid Polym. Sci.* **2008**, 286, 1103.
- [7] P. Bailon, A. Palleroni, C. A. Schaffer, C. L. Spence, W. J. Fung, J. E. Porter, G. K. Ehrlich, W. Pan, Z. X. Xu, M. W. Modi, A. Farid, W. Berthold, *Bioconjugate Chem.* **2001**, 12, 195.
- [8] a) H. Kim, Y. J. Kang, S. Kang, K. T. Kim, *J. Am. Chem. Soc.* **2012**, 134, 4030; b) M. Wang, K. Alberti, S. Sun, C. L. Arellano, Q. Xu, *Angew. Chem., Int. Ed.* **2014**, 53, 2893.
- [9] X. Wang, H. Sun, F. Meng, R. Cheng, C. Deng, Z. Zhong, *Biomacromolecules* **2013**, 14, 2873.
- [10] P. Ghosh, X. Yang, R. Arvizo, Z.-J. Zhu, S. S. Agasti, Z. Mo, V. M. Rotello, *J. Am. Chem. Soc.* **2010**, 132, 2642.
- [11] a) I. I. Slowing, B. G. Trewyn, V. S. Y. Lin, *J. Am. Chem. Soc.* **2007**, 129, 8845; b) E. A. Prasetyanto, A. Bertucci, D. Septiadi, R. Corradini, P. Castro-Hartmann, L. De Cola, *Angew. Chem., Int. Ed.* **2016**, 55, 3323.
- [12] a) J. Chen, J. Ouyang, Q. Chen, C. Deng, F. Meng, J. Zhang, R. Cheng, Q. Lang, Z. Zhong, *ACS Appl. Mater. Interfaces* **2017**, 9, 24140; b) K. Dutta, D. Hu, B. Zhao, A. E. Ribbe, J. Zhuang, S. Thayumanavan, *J. Am. Chem. Soc.* **2017**, 139, 5676; c) I. Nearmtu, A. G. Rusu, A. Diaconu, L. E. Nita, A. P. Chiriac, *Drug Delivery* **2017**, 24, 539; d) L. Tang, Y. Zheng, M. B. Melo, L. Mabardi, A. P. Castano, Y.-Q. Xie, N. Li, S. B. Kudchodkar, H. C. Wong, E. K. Jeng, M. V. Maus, D. J. Irvine, *Nat. Biotechnol.* **2018**, 36, 707.
- [13] Q. Sun, Z. Zhou, N. Qiu, Y. Shen, *Adv. Mater.* **2017**, 29, 1606628.
- [14] H. He, Y. Chen, Y. Li, Z. Song, Y. Zhong, R. Zhu, J. Cheng, L. Yin, *Adv. Funct. Mater.* **2018**, 28, 1707371.
- [15] a) L. Qian, J. Fu, P. Yuan, S. Du, W. Huang, L. Li, S. Q. Yao, *Angew. Chem., Int. Ed.* **2018**, 57, 1532; b) J. Fu, C. Yu, L. Li, S. Q. Yao, *J. Am. Chem. Soc.* **2015**, 137, 12153.
- [16] a) M. Wang, S. Sun, C. I. Neufeld, B. Perez-Ramirez, Q. B. Xu, *Angew. Chem., Int. Ed.* **2014**, 53, 13444; b) T. Suma, J. Cui, M. Muellner, Y. Ju, J. Guo, M. Hu, F. Caruso, *ACS Macro Lett.* **2015**, 4, 160.
- [17] a) A. J. Kirby, P. W. Lancaster, *J. Chem. Soc., Perkin Trans. 2* **1972**, 2, 1206; b) S. Su, F.-S. Du, Z.-C. Li, *Org. Biomol. Chem.* **2017**, 15, 8384.
- [18] a) S. Kang, Y. Kim, Y. Song, J. U. Choi, E. Park, W. Choi, J. Park, Y. Lee, *Bioorg. Med. Chem. Lett.* **2014**, 24, 2364; b) Q. Zhou, Y. Hou, L. Zhang, J. Wang, Y. Qiao, S. Guo, L. Fan, T. Yang, L. Zhu, H. Wu, *Theranostics* **2017**, 7, 1806.
- [19] a) Y. Lee, T. Ishii, H. Cabral, H. J. Kim, J.-H. Seo, N. Nishiyama, H. Oshima, K. Osada, K. Kataoka, *Angew. Chem., Int. Ed.* **2009**, 48, 5309; b) Z. X. Zhou, Y. Q. Shen, J. B. Tang, M. H. Fan, E. A. Van Kirk, W. J. Murdoch, M. Radosz, *Adv. Funct. Mater.* **2009**, 19, 3580; c) J. Z. Du, X. J. Du, C. Q. Mao, J. Wang, *J. Am. Chem. Soc.* **2011**, 133, 17560; d) H. Murata, S. Carmali, S. L. Baker, K. Matyjaszewski, A. J. Russell, *Nat. Commun.* **2018**, 9, 845; e) Z. Zhang, X. Zhang, X. Xu, Y. Li, Y. Li, D. Zhong, Y. He, Z. Gu, *Adv. Funct. Mater.* **2015**, 25, 5250; f) S. Chen, L. Rong, Q. Lei, P.-X. Cao, S.-Y. Qin, D.-W. Zheng, H.-Z. Jia, J.-Y. Zhu, S.-X. Cheng, R.-X. Zhuo, X.-Z. Zhang, *Biomaterials* **2016**, 77, 149; g) X. Guan, Y. Li, Z. Jiao, L. Lin, J. Chen, Z. Guo, H. Tian, X. Chen, *ACS Appl. Mater. Interfaces* **2015**, 7, 3207.
- [20] Y. Lee, T. Ishii, H. J. Kim, N. Nishiyama, Y. Hayakawa, K. Itaka, K. Kataoka, *Angew. Chem., Int. Ed.* **2010**, 49, 2552.
- [21] a) B. Zhivotovsky, S. Orrenius, O. T. Brustugun, S. O. Doskeland, *Nature* **1998**, 391, 449; b) M. Huettemann, P. Pecina, M. Rainbolt, T. H. Sanderson, V. E. Kagan, L. Samavati, J. W. Doan, I. Lee, *Mitochondrion* **2011**, 11, 369.
- [22] L. E. Yandek, A. Pokorny, A. Floren, K. Knoelke, U. Langel, P. F. F. Almeida, *Biophys. J.* **2007**, 92, 2434.
- [23] X. Zhang, S. Malhotra, M. Molina, R. Haag, *Chem. Soc. Rev.* **2015**, 44, 1948.
- [24] a) M. Yan, J. Ge, Z. Liu, P. Ouyang, *J. Am. Chem. Soc.* **2006**, 128, 11008; b) J. Mendez, M. M. Cruz, Y. Delgado, C. M. Figueroa, E. A. Orellano, M. Morales, A. Montegudo, K. Griebenow, *Mol. Pharmaceutics* **2014**, 11, 102; c) Y. Hou, J. Yuan, Y. Zhou, J. Yu, H. Lu, *J. Am. Chem. Soc.* **2016**, 138, 10995.
- [25] J. M. Chen, C. Ferec, *Pancreas* **2000**, 21, 57.
- [26] R. E. Childs, W. G. Bardsley, *Biochem. J.* **1975**, 145, 93.